Research Article | Vol. 8, No. 11 | 1 Nov 2017 | BIOMEDICAL OPTICS EXPRESS 5139

Biomedical Optics EXPRESS

Speckle variance OCT for depth resolved assessment of the viability of bovine embryos

S. CAUJOLLE,[1,2,4,*] R. CERNAT,[1,4] G. SILVESTRI,[3,4] M. J. MARQUES,[1] A. BRADU,[1] T. FEUCHTER,[2] G. ROBINSON,[3] D. K. GRIFFIN,[3] AND A. PODOLEANU[1]

[1]*Applied Optics Group, School of Physical Sciences, University of Kent, Canterbury, CT2 7NH, UK*
[2]*NKT Photonics A/S, Blokken 84, 3460 Birkerød, Zealand, Denmark*
[3]*School of Biosciences, University of Kent, Canterbury, CT2 7AF, UK*
[4]*contributed equally to this work*
[*]*smcc4@kent.ac.uk*

Abstract: The morphology of embryos produced by *in vitro* fertilization (IVF) is commonly used to estimate their viability. However, imaging by standard microscopy is subjective and unable to assess the embryo on a cellular scale after compaction. Optical coherence tomography is an imaging technique that can produce a depth-resolved profile of a sample and can be coupled with speckle variance (SV) to detect motion on a micron scale. In this study, day 7 post-IVF bovine embryos were observed either short-term (10 minutes) or long-term (over 18 hours) and analyzed by swept source OCT and SV to resolve their depth profile and characterize micron-scale movements potentially associated with viability. The percentage of *en face* images showing movement at any given time was calculated as a method to detect the vital status of the embryo. This method could be used to measure the levels of damage sustained by an embryo, for example after cryopreservation, in a rapid and non-invasive way.

© 2017 Optical Society of America

OCIS codes: (110.4500) Optical coherence tomography; (170.1420) Biology; (110.4153) Motion estimation and optical flow; (170.3880) Medical and biological imaging; (030.6140) Speckle.

References and links

1. P. Holm, N. N. Shukri, G. Vajta, P. Booth, C. Bendixen, and H. Callesen, "Developmental kinetics of the first cell cycles of bovine in vitro produced embryos in relation to their in vitro viability and sex," Theriogenology **50**(8), 1285–1299 (1998).
2. I. Boiso, A. Veiga, and R. G. Edwards, "Fundamentals of human embryonic growth in vitro and the selection of high-quality embryos for transfer," Reprod. Biomed. Online **5**(3), 328–350 (2002).
3. G. M. Lindner and R. W. Wright, Jr., "Bovine embryo morphology and evaluation," Theriogenology **20**(4), 407–416 (1983).
4. A. Van Soom, B. Mateusen, J. Leroy, and A. De Kruif, "Assessment of mammalian embryo quality: what can we learn from embryo morphology?" Reprod. Biomed. Online **7**(6), 664–670 (2003).
5. G. A. Bo and R. J. Mapletoft, "Evaluation and classification of bovine embryos," Anim. Reprod. **10**(3), 344–348 (2013).
6. M. Alikani, J. Cohen, G. Tomkin, G. J. Garrisi, C. Mack, and R. T. Scott, "Human embryo fragmentation in vitro and its implications for pregnancy and implantation," Fertil. Steril. **71**(5), 836–842 (1999).
7. T. Somfai, Y. Inaba, Y. Aikawa, M. Ohtake, S. Kobayashi, K. Konishi, and K. Imai, "Relationship between the length of cell cycles, cleavage pattern and developmental competence in bovine embryos generated by in vitro fertilization or parthenogenesis," J. Reprod. Dev. **56**(2), 200–207 (2010).
8. C. Racowsky, P. Kovacs, and W. P. Martins, "A critical appraisal of time-lapse imaging for embryo selection: where are we and where do we need to go?" J. Assist. Reprod. Genet. **32**(7), 1025–1030 (2015).
9. M. R. Hee, C. A. Puliafito, C. Wong, J. S. Duker, E. Reichel, J. S. Schuman, E. A. Swanson, and J. G. Fujimoto, "Optical coherence tomography of macular holes," Ophthalmology **102**(5), 748–756 (1995).
10. D. Ruminski, B. L. Sikorski, D. Bukowska, M. Szkulmowski, K. Krawiec, G. Malukiewicz, L. Bieganowski, and M. Wojtkowski, "OCT angiography by absolute intensity difference applied to normal and diseased human retinas," Biomed. Opt. Express **6**(8), 2738–2754 (2015).
11. A. Federici, H. S. da Costa, J. Ogien, A. K. Ellerbee, and A. Dubois, "Wide-field, full-field optical coherence microscopy for high-axial-resolution phase and amplitude imaging," Appl. Opt. **54**(27), 8212–8220 (2015).

#303096 https://doi.org/10.1364/BOE.8.005139
Journal © 2017 Received 25 Jul 2017; revised 14 Sep 2017; accepted 24 Sep 2017; published 20 Oct 2017

Biomedical Optics EXPRESS

12. I. Gorczynska, J. V. Migacz, R. J. Zawadzki, A. G. Capps, and J. S. Werner, "Comparison of amplitude-decorrelation, speckle-variance and phase-variance OCT angiography methods for imaging the human retina and choroid," Biomed. Opt. Express **7**(3), 911–942 (2016).
13. M. S. Mahmud, D. W. Cadotte, B. Vuong, C. Sun, T. W. Luk, A. Mariampillai, and V. X. Yang, "Review of speckle and phase variance optical coherence tomography to visualize microvascular networks," J. Biomed. Opt. **18**(5), 50901 (2013).
14. A. Mariampillai, M. K. K. Leung, M. Jarvi, B. A. Standish, K. Lee, B. C. Wilson, A. Vitkin, and V. X. D. Yang, "Optimized speckle variance OCT imaging of microvasculature," Opt. Lett. **35**(8), 1257–1259 (2010).
15. Y. Huang, Q. Zhang, M. R. Thorell, L. An, M. K. Durbin, M. Laron, U. Sharma, G. Gregori, P. J. Rosenfeld, and R. K. Wang, "Swept-source OCT angiography of the retinal vasculature using intensity differentiation-based optical microangiography algorithms," Ophthalmic Surg. Lasers Imaging Retina **45**(5), 382–389 (2014).
16. W. Drexler, U. Morgner, F. X. Kärtner, C. Pitris, S. A. Boppart, X. D. Li, E. P. Ippen, and J. G. Fujimoto, "In vivo ultrahigh-resolution optical coherence tomography," Opt. Lett. **24**(17), 1221–1223 (1999).
17. I. V. Larina, K. Furushima, M. E. Dickinson, R. R. Behringer, and K. V. Larin, "Live imaging of rat embryos with Doppler swept-source optical coherence tomography," J. Biomed. Opt. **14**(5), 050506 (2009).
18. K. Karnowski, A. Ajduk, B. Wieloch, S. Tamborski, K. Krawiec, M. Wojtkowski, and M. Szkulmowski, "Optical coherence microscopy as a novel, non-invasive method for the 4D live imaging of early mammalian embryos," Sci. Rep. **7**(1), 4165 (2017).
19. J. G. Zheng, D. Lu, T. Chen, C. Wang, N. Tian, F. Zhao, T. Huo, N. Zhang, D. Chen, W. Ma, J. L. Sun, and P. Xue, "Label-free subcellular 3D live imaging of preimplantation mouse embryos with full-field optical coherence tomography," J. Biomed. Opt. **17**(7), 070503 (2012).
20. P. Holm, P. J. Booth, M. H. Schmidt, T. Greve, and H. Callesen, "High bovine blastocyst development in a static in vitro production system using SOFaa medium supplemented with sodium citrate and myo-inositol with or without serum-proteins," Theriogenology **52**(4), 683–700 (1999).
21. R. Cernat, A. Bradu, N. M. Israelsen, O. Bang, S. Rivet, P. A. Keane, D. G. Heath, R. Rajendram, and A. Podoleanu, "Gabor fusion master slave optical coherence tomography," Biomed. Opt. Express **8**(2), 813–827 (2017).
22. A. G. Podoleanu and A. Bradu, "Master-slave interferometry for parallel spectral domain interferometry sensing and versatile 3D optical coherence tomography," Opt. Express **21**(16), 19324–19338 (2013).
23. S. Rivet, M. Maria, A. Bradu, T. Feuchter, L. Leick, and A. Podoleanu, "Complex master slave interferometry," Opt. Express **24**(3), 2885–2904 (2016).
24. I. V. Larina, S. Ivers, S. Syed, M. E. Dickinson, and K. V. Larin, "Hemodynamic measurements from individual blood cells in early mammalian embryos with Doppler swept source OCT," Opt. Lett. **34**(7), 986–988 (2009).
25. N. Sudheendran, S. H. Syed, M. E. Dickinson, I. V. Larina, and K. V. Larin, "Speckle variance OCT imaging of the vasculature in live mammalian embryos," Laser Phys. Lett. **8**(3), 247 (2011).
26. K. S. Richter, D. C. Harris, S. T. Daneshmand, and B. S. Shapiro, "Quantitative grading of a human blastocyst: optimal inner cell mass size and shape," Fertil. Steril. **76**(6), 1157–1167 (2001).
27. A. van Soom, M. T. Ysebaert, and A. de Kruif, "Relationship between timing of development, morula morphology, and cell allocation to inner cell mass and trophectoderm in in vitro-produced bovine embryos," Mol. Reprod. Dev. **47**(1), 47–56 (1997).
28. A. H. Handyside and S. Hunter, "A rapid procedure for visualising the inner cell mass and trophectoderm nuclei of mouse blastocysts in situ using polynucleotide-specific fluorochromes," J. Exp. Zool. **231**(3), 429–434 (1984).
29. G. A. Thouas, N. A. Korfiatis, A. J. French, G. M. Jones, and A. O. Trounson, "Simplified technique for differential staining of inner cell mass and trophectoderm cells of mouse and bovine blastocysts," Reprod. Biomed. Online **3**(1), 25–29 (2001).
30. K. Hardy, A. H. Handyside, and R. M. Winston, "The human blastocyst: cell number, death and allocation during late preimplantation development in vitro," Development **107**(3), 597–604 (1989).
31. H. Stinshoff, S. Wilkening, A. Hanstedt, K. Brüning, and C. Wrenzycki, "Cryopreservation affects the quality of in vitro produced bovine embryos at the molecular level," Theriogenology **76**(8), 1433–1441 (2011).
32. L. Zarnescu, M. Abeyta, T. M. Baer, B. Behr, and A. K. Ellerbee, "Assessment of imaging parameters correlated with the effects of cryopreservation on embryo development," Optical Methods in Developmental Biology II, Proc. SPIE **8953**, 89530F (2014).
33. L. Zarnescu, M. C. Leung, M. Abeyta, H. Sudkamp, T. Baer, B. Behr, and A. K. Ellerbee, "Label-free characterization of vitrification-induced morphology changes in single-cell embryos with full-field optical coherence tomography," J. Biomed. Opt. **20**(9), 096004 (2015).

1. Introduction

After fertilization, mammalian zygotes undertake a series of rapid mitotic divisions known as cleavage events which bring them from the original 1 cell to 16-32 cells. In cattle, this phase has a duration of approximately 4 days, after which the embryo undergoes the process of compaction during which it appears as a tight cluster of cells with hardly any distinguishable inter-cellular borders. Between day 6 and 7 after fertilization, as the embryo continues to grow, a liquid filled cavity develops, termed as blastocoel, whilst the embryo is referred to as

Biomedical Optics EXPRESS

the blastocyst. By the time the embryo reaches the blastocyst stage, its cells have formed two distinct populations: a thin outer layer known as trophectoderm and a compact cluster known as the inner cell mass [1]. A normal bovine blastocyst is presented in Fig. 1.

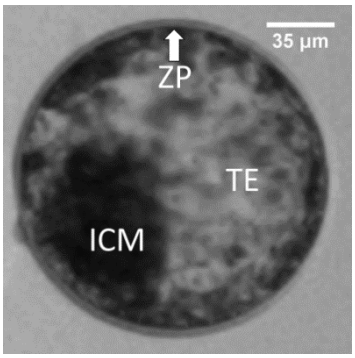

Fig. 1. A typical bovine blastocyst produced *in vitro* using the same method described under section 2.1. ICM: inner cell mass, TE: trophectoderm, ZP: zona pellucida. The embryo can be imagined as a liquid filled sphere. The ICM forms a discrete unit and is attached to the sphere's internal surface, while the surface itself is formed by the thin TE cell layer. Additionally, an outer proteic shell, the ZP (arrow), encapsulates the whole embryo. The image was acquired by a Nikon Eclipse TE200 inverted modulation contrast microscope at x200 total magnification and by using an RI DC2 camera and its dedicated software RI Viewer.

In order to establish a pregnancy, bovine blastocysts produced by *in vitro* fertilization (IVF) are transferred into recipient animals, but the eligibility for transfer requires assessment of the viability of each candidate embryo. Evaluation of the embryo morphology, as a method to estimate its viability, has found wide use in human IVF [2] and the principle that the transfer of embryos of better morphology leads to higher pregnancy rates has long been validated in cattle [3]. One of the most substantial differences between human and bovine embryos, however, is that the latter are made opaque by the accumulation of lipid droplets in their cytoplasm, which makes the embryo harder to assess though conventional methods [4]. Commonly, bovine blastocysts produced by IVF are screened morphologically at x50 to x100 magnification using a stereomicroscope [5]. Whilst this level of investigation is simple and non-invasive, it is also highly subjective, gives little indication of intracellular activity [4], and is unable to quantify accurately the percentage of fragmentation (amount of sub-cellular, non-viable material) in the embryo which is known to affect its viability [6].

To support the morphological assessment of embryos and in an attempt to provide a better prediction of viability, time-lapse systems have been introduced [7]. Although widespread, the use of these systems has failed to produce obvious benefits due to the lack of a stringent correlation between the morphokinetic parameters measured and clinical pregnancy outcomes [8]. Time-lapse systems also present the disadvantages of a long time required to complete an assessment and of a poor depth of view. The second problem is made worse in post-compaction embryos like blastocysts and in bovine embryos generally due to their unfavourable lipid distribution [4]. An example of these limitations is given in Fig. 2, showing that protracted time-lapse observation is likely required to detect any changes in embryo morphology while at the same time, information on the different optical planes of the embryo is likely lost.

Therefore, there is scope for the development and application of new imaging modalities able to resolve the embryo structure in full depth and provide for a rapid and non-subjective assessment of viability.

Optical Coherence Tomography (OCT) is a non-invasive optical method developed in the 1990s that has historically found most applications in ophthalmology [9]. It can create structural images of biological tissues with high axial and transverse resolution providing cross-sectional 2D maps in the (x,z) or (y,z) planes (B-scans) and *en face* 2D maps in the

Biomedical Optics EXPRESS

(x,y) plane (C-scan), where x and y coordinates are measured along the lateral directions of the sample and z coordinate is measured along its depth.

Moreover, recent advancements have also allowed for the acquisition of functional images, one example being Optical Coherence Tomography Angiography (OCTA) which is used to differentiate moving blood cells from stationary features. The detection is possible due to algorithms like Speckle Variance (SV) analysis which can quantify the changes in the speckle pattern of a sample associated with movement [10–15].

OCT has already found some limited application in developmental biology in model organisms like *Xenopus laevis* [16], and *Rattus norvegicus* [17]. Recently, high-resolution intracellular imaging on live mouse and pig oocytes and embryos has been reported [18]. In this context, the fundamental advantages of OCT are its ability to image embryos without labels, and its use of low power light sources as compared to confocal systems. The use of low power optical beams reduces the chance of damaging the embryo during observation [18, 19]. However, no study so far has applied the motion detection principles of OCTA to early stage embryos, like blastocysts, to assess their viability.

In this study, an OCT system was used to produce a full depth structural characterization of a day 7 post IVF blastocyst and display its 3-D models. Moreover, to test whether kinetic differences could be measured between live and dead embryos, micron-scale movements were measured with the SV method to enable quantitative analysis of embryo viability over time.

Fig. 2. Images of a day 7 bovine blastocyst at different time points after insemination. The images were acquired by phase contrast microscopy at x200 magnification using a time-lapse system PrimoVision Evo (Vitrolife). Completing a viability assessment is likely to require protracted observation as the general morphology of the embryo changes very little over time. Scale bar = 50 µm.

2. Materials and methods

2.1 Preparation of bovine embryos

Bovine blastocysts were produced *in vitro* following a previously described method [20]. Briefly, oocytes were collected from abattoir material and *in vitro* matured, then fertilized with frozen/thawed sperm (Semex). The resulting embryos were then cultured in Synthetic Ovarian Fluid (SOF) medium droplets until they reached the blastocyst stage 7 days post-IVF. Five of the resulting blastocysts were monitored by OCT over short-term observation of several minutes whereas one embryo was monitored over long-term observation (exceeding 18 hours).

2.2 Set-up

The OCT system used is schematically presented in Fig. 3. A swept source at 1310 nm center wavelength (Axsun Technologies), 100 kHz sweep rate, 12 mm coherence length, 106 nm FWHM bandwidth in the range (1256.6 nm–1362.8 nm) [21] is used. The source is connected to a 2 × 2 fiber coupler (C1) with an 80:20 ratio which splits 80% of the power towards the reference arm and 20% of the reference power towards the sample arm. In the sample arm, light is collimated through lens L1 and directed to a pair of galvanometer scanners which, via the imaging lens L2, scan the beam laterally in the (x,y) plane. Light from the reference and

Biomedical Optics EXPRESS

sample arms are combined in the 50:50 fiber coupler C2. The output ports from C2 are routed to a balanced photo-detector (Thorlabs Model PDB460C, DC 200 MHz). A 12-bit waveform digitizer (AlazarTech ATS9350 - 500 MS/s) digitizes the output signal which is processed using an "in-house" acquisition software written in LabVIEW (National Instruments). This software calculates 500 *en face* images from 500 depths and delivers a real-time compound display of two cross section OCT images, 9 *en face* OCT images and a summed voxel projection (SVP) image, all made possible due to the use of Master-Slave interferometry protocol [21–23]. The combined rendering of the 12 such images is updated every 0.8 s. The depth interval between the 9 selected depth positions is chosen to cover the axial range of the full embryo. Images are produced from 200x200 lateral pixels. The axial resolution was measured to be approximately 15 µm in air and the transverse resolution approximately 4.2 µm.

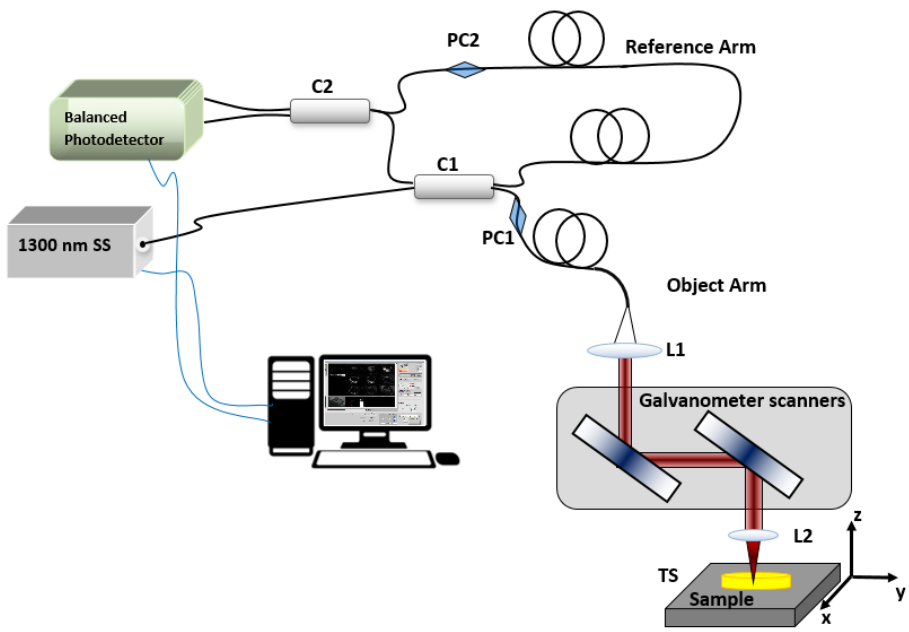

Fig. 3. OCT set-up. SS: swept source; C1, C2: directional optical couplers, PC1, PC2: polarization controllers, L1, L2: lenses, TS: x,y,z translation stage to position the sample.

2.3 Image acquisition and speckle variance (SV) analysis

The embryos are placed on a Petri dish. Then the dish is adjusted laterally and vertically, using the translation stage, TS, by monitoring the SVP image. Initially, the differential distance between the 9 *en face* images in the display is adjusted approximately based on an estimated embryo thickness. While monitoring the two cross section OCT images, the reference arm length is adjusted in order to position the cross sections of the embryos in their central region.

To characterize the structure and the progressive loss of viability of the embryos, cross section images and *en face* images were acquired over short and long-term observation. For short-term observation, 5 embryos were observed for 10 minutes and a full set of data was acquired every minute. For long-term observation, the embryo was observed until it ceased all motion (18 hours), acquiring a set of data every minute for 10 min followed by 20 min of rest; the no-motion measurement was confirmed by another observation performed after a further 8 hours. The SV analysis was performed as described before [10–14] on successive *en face* images at 1 min intervals. The Speckle Variance for each lateral pixel (j,k) is defined as:

Biomedical Optics EXPRESS

$$SV(i,j,k)=\frac{1}{N}\sum_{i=1}^{N}\left(I(i,j,k)-\frac{1}{N}\sum_{i=1}^{N}I(i,j,k)\right)^2 \quad (1)$$

In (1), I is the strength of the OCT signal at each pixel, N is the total number of *en face* images considered for the calculation which in our case is N = 2 and the index i is the *en face* image concerned, respectively. The calculation was over j and k, i.e. over 200 by 200 pixels, leading to a 2D motion map of similar size. The lateral size of *en face* images is 230 µm by 230 µm. The SV values represent the variance calculated over two successive images with a time lapse equal to 1 min. The larger the variability, the larger the SV. A SV value equal to 0 means that images are identical and no motion is detected. To compensate the effects of Brownian motion, image sets from a dead embryo were also acquired and used to establish a minimum speckle variance value (threshold) for each pixel. In the final display of motion maps, all pixel values whose SV was below this threshold were assigned zero values. Moreover, to produce a quantitative assessment of motion, a parameter "quantity of movement" was calculated as the summation of all pixel values from the motion map.

3. Results

Overall, 5 live bovine blastocysts were observed for 10 minutes (short-term observation) and 1 bovine blastocyst was observed for over 18 hours (long-term observation). During the assessment, 12 structural images were displayed in real time in the form of SVP, 2 x cross sectional images and 9 x *en face* images. In Fig. 4, an example of the acquisition display is given.

Biomedical Optics EXPRESS

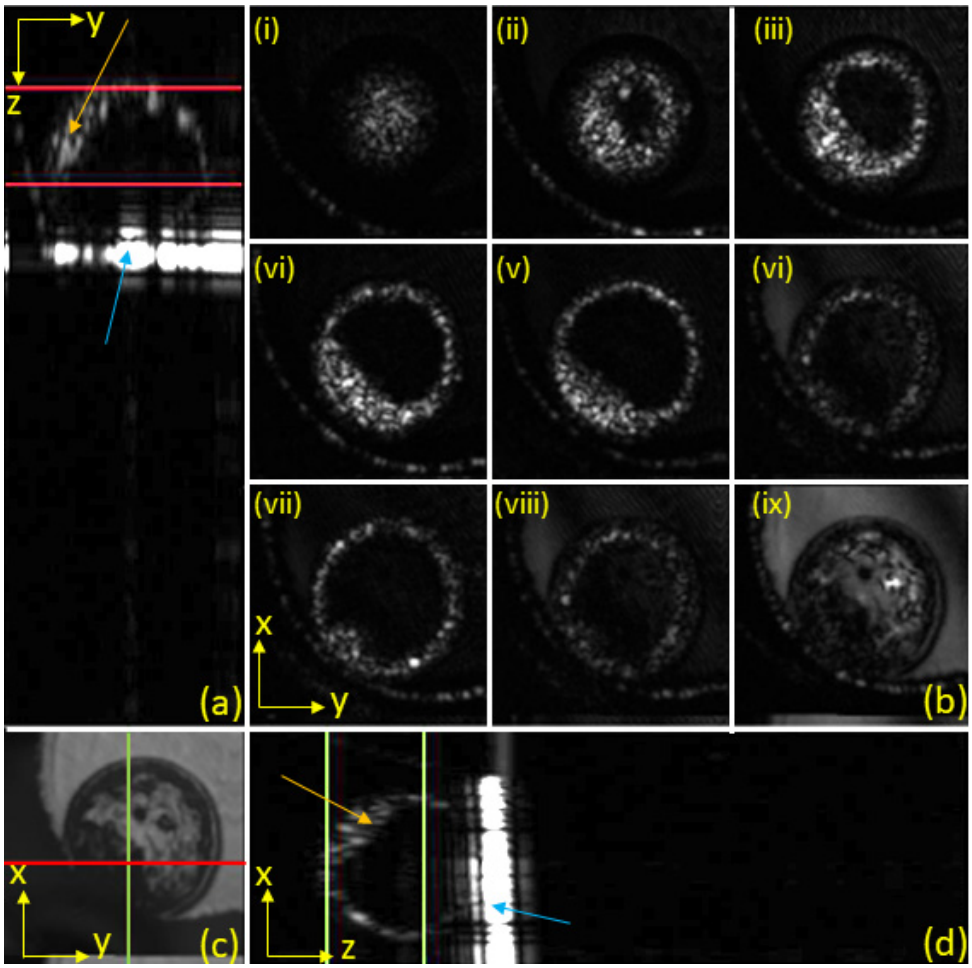

Fig. 4. Screen-shot of the "in-house" Master/Slave software used for image guidance. Three categories of images are displayed simultaneously and in real time in each raster: 2x cross section images, 9x *en face* images and a SVP. (a) Cross section along the red line (plane (z,y)) in the SVP image, (b) (i-ix) *en face* images, (c) SVP and (d) cross section image along the green line (plane (x,z)) in the SVP image. To cover the whole depth of the embryo, 9 *en face* images (i – ix) are shown over a total depth of 225 µm, separated by a depth interval of 25 µm (measured in air). All images are represented on a linear scale. Blue arrows indicate the glass plate and the orange arrow indicates the embryo shape. The lateral size of images is 230 µm and the axial range of the cross sections is 1 mm (measured in air).

3.1 Blastocyst 3D reconstruction and structural imaging

En face images were used to create a 3D volume of the embryo as shown in Fig. 5 and could be used to identify two separate structural entities forming a blastocyst, namely a ring of outer cells (trophectoderm) and a discrete mass of cells in the inside (inner cell mass). The volume allowed by the "in-house" acquisition software written in LabVIEW software extends over a voxel size of 200x200x500 pixels.

Biomedical Optics EXPRESS

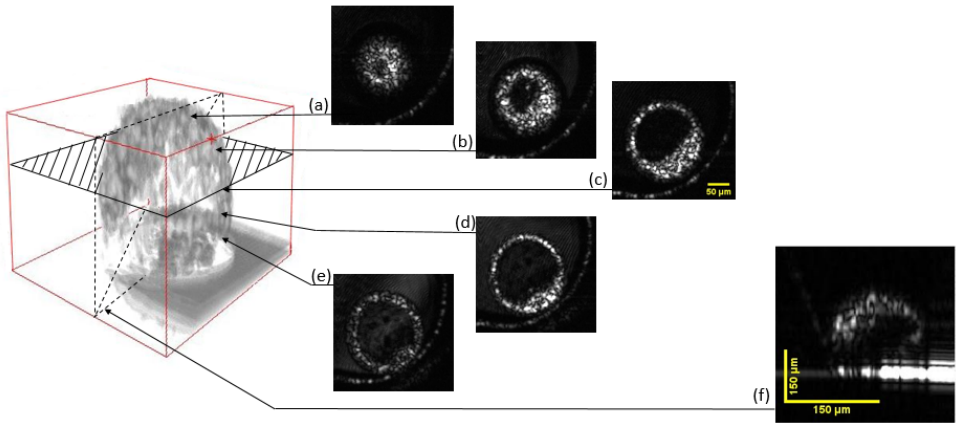

Fig. 5. 3D display of a day 7-post *in vitro* fertilization bovine embryo. *En face* images at different depths from the top embryo surface (a) 25µm, (b) 75µm, (c) 150µm, (d) 225µm and (e) 300µm (all measured in air) at the beginning of the experiment, scale bar = 50µm. (f) cross section view over 500 µm in depth (measured in air), scale bar = 150 µm x 150 µm.

By varying the differential distance between the depths, the axial range was adjusted as such, that the embryo covers 300 depths. Therefore, the size of the volume displayed in Fig. 5 is 200x200x300. Moreover, the shape of the inner cell mass could be clearly distinguished in the 3D reconstruction potentially providing information on its compactness, size and distribution. As described in the introduction (and also in Fig. 2) a blastocyst stage embryo does not necessarily display large morphological changes over a time period of a few hours when observed by standard microscopy, but it can sometimes display a pulsating behavior whereby the embryo collapses on itself and then re-expands to its full size. In this analysis, the blastocyst appeared to maintain its normal structure over the first 12 h; however, by the 13th hour it started to collapse on itself. From this point on, a faint halo of the same size as the original embryo could be detected by OCT indicating that the blastocyst's zona pellucida maintained its shape and position while the rest of the embryo collapsed. Interestingly, the complete collapse of the blastocyst's inner cavity was observed between 15 and 16 h of culture and this detail would have been impossible to notice with standard microscopy. After this point, however, the embryo failed to re-expand, an observation consistent with an embryo approaching the end of its life. A selection of images acquired over long-term observation is given in Fig. 6(A), showing the first 18 h of culture and an additional image acquired 8 h after complete cessation of embryo motion.

3.2 Micron-scale movement detection by SV and quantity of movement calculation

The SV algorithm was applied to obtain motion maps at each embryo depth to highlight the portions of the embryos in motion during each 1 min interval considered. The analysis could also indicate when the embryo ceased all motion (Fig. 6(B)).

For the 5 embryos selected for the short-term observations, motion maps were calculated using *en face* images from a depth approximately in the middle of each embryo.

Figure 7 shows the maximum speckle variance registered in such maps. Usefully, the maximum value calculated for the dead control embryo was found to be at least 5 times smaller than the average maximum value of any live embryo.

For the next evaluations, a threshold was calculated to differentiate the live embryos from the dead one. This was obtained as the maximum SV extracted from the motion maps evaluated over the whole embryo volume.

In Fig. 8, quantity of movement was calculated at 5 different depths (as indicated) in the same embryo over long-term observation and it was possible to pinpoint at which depth the

Biomedical Optics EXPRESS

embryo maintained movement over time. The calculation included only those pixels out of the 200x200, where the SV exceeded the threshold evaluated above.

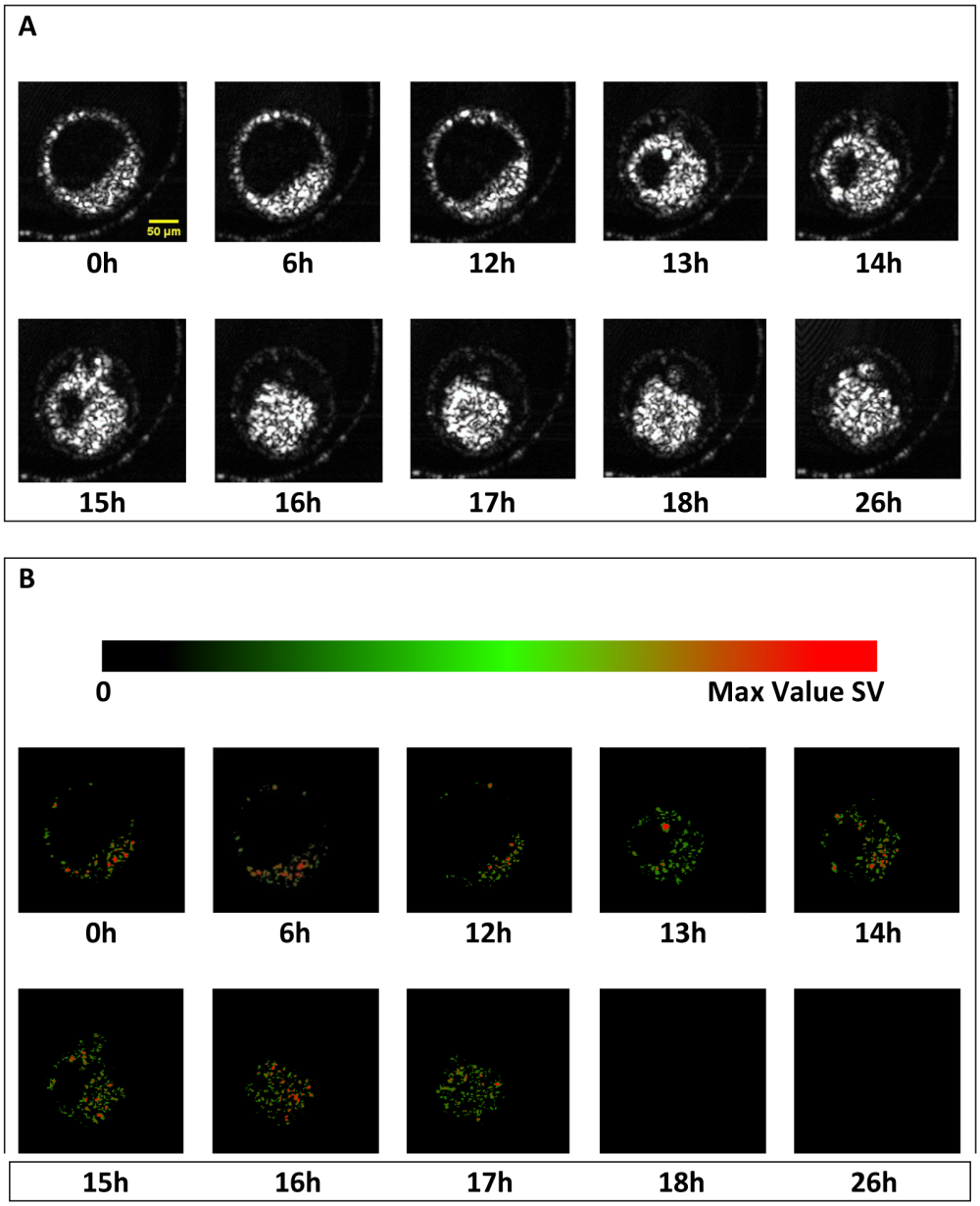

Fig. 6. *En face* images (A) of the embryo over 26 h (actively monitored over the first 18 h) and their SV *en face* display/Motion Map (B) at a fixed depth (150 µm from the top embryo surface measured in air). Scale bar = 50µm. SV value are displayed Red/Green scale. Red represents higher value.

An alternative representation of this information is given in Fig. 9, showing the percentage of *en face* images from the same embryo in which movement could be detected at any given time. The calculation was performed over 300 *en face* images obtained from different depths covering the embryo thickness (i.e. using the same adjustment of axial range as in Fig. 5).

Biomedical Optics EXPRESS

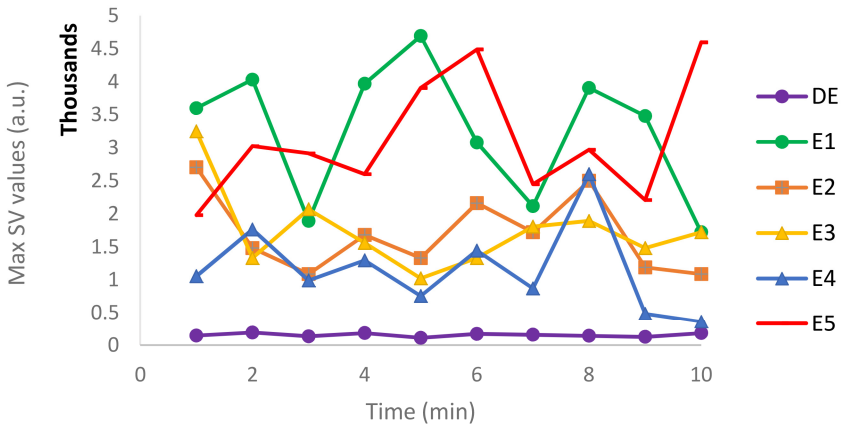

Fig. 7. Maximum value of the Speckle Variance for different embryos over 10 minutes. Embryo 1 – Embryo 5 (E1-E5): Curves representing the quantity of movement for live embryos, DE: Curve for dead embryo.

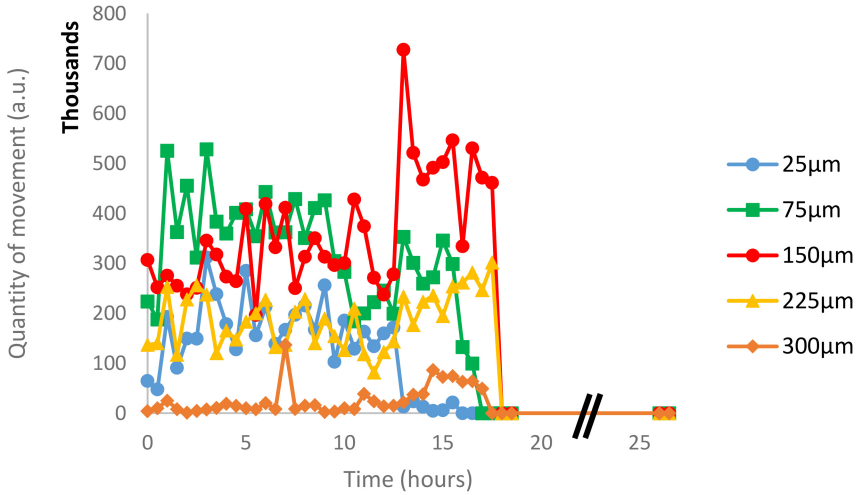

Fig. 8. Quantity of movement (for the embryo 5 in Fig. 6) at superficial (25 µm and 300 µm, middle (75 µm and 225 µm) and central depth (150 µm) over long-term observation.

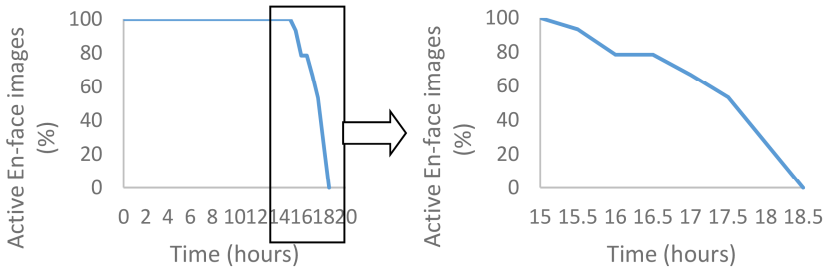

Fig. 9. Percentage of number of *en face* images displaying SV values above threshold at any given time for an embryo (number 5 in Fig. 7) over long-term observation. The downward trend is expanded on the right hand to better display the decreasing motion of the embryo over time.

Biomedical Optics EXPRESS

4. Discussion

To date, a limited number of reports have focused on applying functional OCT imaging to study early mammalian embryos [18, 24, 25]. However, to our best knowledge, this is the first time OCT and SV have been applied to a day 7 post-IVF mammalian embryo to resolve its 3D structure and quantify micron-scale movement.

As seen in Fig. 5, OCT can be successfully used to identify the key structures within the bovine blastocyst. Additionally, motion maps can be produced (Fig. 6(B)) to detect motion in the areas of the blastocyst which are populated with cells.

Over short-term observation, all live embryos consistently displayed higher SV values (Fig. 7) when compared with dead controls suggesting that a live embryo is likely to possess levels of intracellular activity detectable by OCT.

However, the interpretation of the motion measurement became more complex during long-term observation. As shown in Fig. 6(A), the embryo had collapsed on itself after 12 h of culture. This is an expected behavior for a blastocyst approaching the end of its life. As shown in Fig. 8, this was associated with a surge in movement around the median portion of the embryo at a depth of 150 µm. One possible explanation for this behavior is that the SV measurement is sensitive at the same time to both genuine intracellular movement and to mechanical movement of the blastocyst's tissues caused by the deflation of its internal cavity and that the summation of these two movements caused the spark detected. Indeed, while the embryo could safely be declared dead after 18 h of culture, the actual cessation of biochemical activity within it could have happened at an earlier time point between 15 and 18 hours. On one hand, non-blank motion maps were obtained between 17 and 18 hours of culture after the complete disappearance of the embryo's blastocoel when mechanical motion seemingly came to an end, suggesting that the embryo more likely ceased all biochemical activity around the 18th hour mark. On the other hand, this might not be the only possible interpretation as spontaneous decaying processes, not necessarily linked with intra-cellular activity, could have been detected instead. However, these type of movements were not present in the dead controls. Therefore, based on the comments above, whilst the decaying trend in Fig. 9 expresses the attenuation of motion inside the embryo, it cannot be used to predict the exact time of the embryo's death.

As portrayed in Fig. 8, the embryo did not behave consistently across its depth from a kinetic point of view over long-term functional observation. This finding is not necessarily surprising since it is known that cells or cell groups in a blastocyst can become fragmented or even die [30]. This is also known to happen in embryos that are cryopreserved. Indeed, the cryopreservation of an embryo in liquid nitrogen is a standard procedure, however not all embryos survive the freeze thawing process and those that do are likely to suffer from various levels of damage [31]. Cryodamage assessment on a per embryo basis is very challenging due to the invasive nature of the tests available. Very few papers have used OCT to investigate cryodamage in embryos [32, 33] and none of them studied blastocyst stage embryos which are widely cryopreserved in both human and animal IVF systems. The SV analysis here described could become a useful tool to quantify the level of damage sustained by cryopreserved embryos within minutes of thawing and without a need for extended culture. The results of this assessment would be easy to interpret since they would simply take the form of percentages of *en face* images in motion, as shown in Fig. 8.

5. Conclusions

We anticipate that in future studies, OCT, due to its potential submicron axial resolution, could be used to obtain precise measurements of the shape and volume of a blastocyst's inner cell mass, since these parameters have been shown to correlate well with implantation rates when measured by conventional microscopy [26]. In a similar way, OCT can be used to measure non-invasively the volume of a blastocyst's trophectoderm to obtain another metric

Biomedical Optics EXPRESS

of embryo quality: the trophectoderm/inner cell mass ratio [27], an assessment that currently implies the destruction of the embryo with standard methods [28, 29].

The assessment of the percentage of *en face* images in active motion could also be expanded to take into account that, due to the spherical nature of the embryo, not all the *en face* images contain the same number of cells so that a proportion of actively moving embryo volume could be calculated instead. This refinement can be conducted to accurately measure the percentage of fragmentation (intended as non-viable material) present in an embryo, a metric closely associated with viability which is currently estimated subjectively [6].

In conclusion, OCT and SV analysis hold promise to become useful tools for the rapid identification of embryos with poor viability for example after freeze/thawing. The proper adjustment of the embryo prior to measurements based on the *en face* direct view of the Master Slave OCT method further facilitates the procedure.

Funding

S. Caujolle, A.Podoleanu and T. Feuchter acknowledge the UBAPHODESA Marie Curie European Industrial Doctorate 607627. M. J. Marques and A. Podoleanu acknowledge the ERC Proof-of-Concept`AMEFOCT' 680879. R. Cernat and A. Podoleanu are supported by the NIHR Biomedical Research Centre (BRC) at Moorfields Eye Hospital NHS Foundation Trust, UCL Institute of Ophthalmology. G. Silvestri acknowledges the University of Kent for his PhD support. M. J. Marques and A. Bradu acknowledge the EPSRC `REBOT' EPN0192291 project. A. Podoleanu is also supported by the Royal Society Wolfson Research Merit Award. D.K. Griffin acknowledges the Innovate UK grant 10189.

Disclosures

(P) A. Podoleanu and A. Bradu are co-inventors of Master Slave patents assigned to the University of Kent. The authors declare that there are no conflicts of interests related to this article.